Int. J. Electrochem. Sci., 10 **(2015)** 10668 - 10676

International Journal of
ELECTROCHEMICAL
SCIENCE
www.electrochemsci.org

Biosynthesis of SnO_2 Nanoparticles by Fig (*Ficus Carica*) Leaf Extract for Electrochemically Determining Hg(II) in Water Samples

Junjie Hu

College of Plant Science, Jinlin Agricultural Science and Technology University Jinlin 132101, China.
E-mail: Junjie_hu@yahoo.com

Received: 31 August 2015 / *Accepted:* 10 October 2015 / *Published:* 4 November 2015

Biosynthesis of stannic oxide nanoparticles (SnO_2 NPs) was achieved in an aqueous mixture of fig (*Ficus carica*) leaf extract and Tin(II) chloride solution at 80°C. The synthesized SnO_2 NPs were characterized by various techniques. Results revealed that the biomolecules in the *Ficus cairca* could act as the template for reduction and stabilization of SnO_2 NPs. We successfully used the biosynthesized SnO_2 NPs as electrode modifier for electrochemically detection of Hg^{2+} in various water samples.

Keywords: Biosynthesis, SnO_2 nanoparticles, Ficus carica, Hg^{2+}

1. INTRODUCTION

Green synthetic strategic-approach is one of the eco-friendly method for preparing nanoparticles. Synthesis of nanomaterials using biosynthesis over chemical synthesis could avoid many problems because the synthesis method does not use any toxic reagent in the preparation method. Three types of materials are commonly used in the biosynthesis process, including enzymes [1], microorganisms [2] and plant extracts [3-6]. Among them, synthesis of nanomaterials using plant extracts is the simplest approach because its low cost, abound resource and simple operation requirement. For example, Yuvakkumar and co-workers reported the biosynthesis of ZnO nanocrystals via rambutan (*Nephelium lappaceum* L.) extract [7]. Ajitha and co-workers reported the successful preparation of Ag NPs using *Plectranthus amboinicus* leaf extract [8]. Jayaseelan and co-workers demonstrated the synthesis of gold nanoparticles by *Abelmoschus esculentus* [9].

Stannic oxide (SnO_2) is a common n-type wide-bandgap semiconductor, which is wildly used in many technological applications, such as gas detection [10], battery anode [11-17], photocatalytic

material and thermal conductive material [18, 19]. Wet chemical method is usually used for SnO_2 NPs synthesis [20-22]. Besides, vapour phase process [23, 24], hydrothermal synthesis [25, 26], precipitation method [27] and sonochemical route are also used for SnO_2 NPs synthesis [28]. Even though there are various SnO_2 synthesis methods available, to the authors' best knowledge and review of the literature, the biosynthesis of SnO_2 only reported by using bacterium *Erwinia herbicola* [29, 30]. Therefore, we think the development of a plant mediated SnO_2 NPs synthesis method is valuable because of the plant mediated method has advantages such as cost effective and environmentally friendly.

Ficus carica is a flowering plant in the genus *Ficus*, known as the fig. Recently, fig leaf extract has been found could be used for synthesizing Ag NPs [31]. In this paper, we report for the synthesis of SnO_2 NPs using *Ficus carica* leaf extract. The biosynthesized SnO_2 NPs were tested by a series of techniques. Moreover, the electrochemical property of the biosynthesized SnO_2 NPs was investigated by determining Hg^{2+} in various water samples.

2. EXPERIMENTAL

Ficus carica leaves were collected, taxonomically identified and authenticated by the botanical survey of Hangzhou botanical garden. The plant leaves were cleaned with Milli-Q water. Then, 20 g of *Ficus carica* leaves were blended using a vegetable blender. The leaf extract was collection sonication of the mixture for 30 min. Tin(II) chloride dehydrate ($SnCl_2 \cdot 2H_2O$) and methylene blue (MB) were purchased from Sigma-Aldrich.

For synthesis of SnO_2 NPs, 0.5 M $SnCl_2 \cdot 2H_2O$ solution was prepared with 40 mL water. Then 20 mL *Ficus carica* leaf extract was added to solution and kept under continuous stirring at 80^oC for 24 h. The SnO_2 NPs were then collected with annealing the sample in a furnace at 200^oC for 1 h.

The morphology of samples was characterized using a SEM (ZEISS, SUPRA 55). The particle size of the biosynthesized SnO_2 NPs was measured using a particle size analyzer (SALD-7500nano, SHIMADZU). The crystal phase information of sample was characterized by a XRD with Cu Kα (λ = 0.1546 nm).radiation (D8-Advanced, Bruker). FTIR spectra were collected via a Nicolet 8700 FTIR spectrometer (Thermo).The UV-vis spectra were collected via Perkin Elmer Lambda 950 UV-vis spectrophotometer.

A glassy carbon electrode (GCE) was polished with alumina-water slurry first. For the electrode surface modification, 5 μL of SnO_2 NPs dispersion (1 mg/mL) was dropped onto the GCE and dried at the room temperature. Electrochemical measurements were performed on a CHI430A electrochemical workstation (USA).The DPV measurement was conducted as follow condition: E-conditioning = 0.8 V, Conditioning time = 30 s, E-step = 0.01 V, E-pulse = 0.2 V, Pulse time = 0.03 s, Scan rate = 0.1 V/s

3. RESULTS AND DISCUSSION

The morphology of the biosynthesized SnO_2 NPs was observed by SEM. As shown in Figure 1A, the biosynthesized SnO_2 NPs displays agglomerated spherical shape. The average particle size of

the biosynthesized SnO_2 was determined by particle size analyzer, and found to be 128 nm (Figure 1C). The elemental information of biosynthesized SnO_2 NPs was analyzed by EDX. As shown in the Figure 1B, intensive peak signals of O and Sn were observed in the spectrum, indicating the composition of Sn and O. Besides, the spectrum also exhibits the existence of C, Na and P, which could due to the biomolecules on the surface of the biosynthesized SnO_2 NPs.

The crystal phase of the biosynthesized SnO_2 NPs was analyzed using XRD. Figure 2 shows the XRD pattern of the biosynthesized SnO_2 NPs, which exhibits a series of well-defined diffraction peaks. The diffraction peaks at 27.05°, 37.21°, 38.99°, 52.02°, 54.19°, 58.05°, 61.89°, 65.06°, 65.74°, 69.21°, 72.01° and 78.98° can be indexed to (110), (200), (111), (211), (220), (002), (310), (112), (301), (202) and (321) crystal planes of tetragonal SnO_2 (JCPDS card No. 41-1445). Moreover, the XRD pattern of the biosynthesized SnO_2 NPs also presents the peak at 27.92°, 32.55° and 46.32°, which corresponding to the carbon signals. As mentioned above, the existence of carbon is likely to originate from the organic encapsulation of SnO_2 NPs.

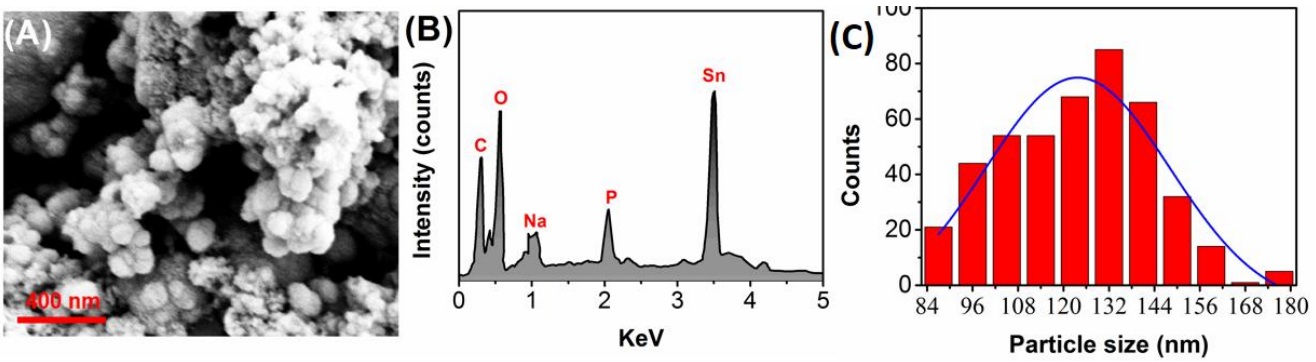

Figure 1. (A) SEM image, (B) EDX spectrum and (C) size distribution of biosynthesized SnO_2.

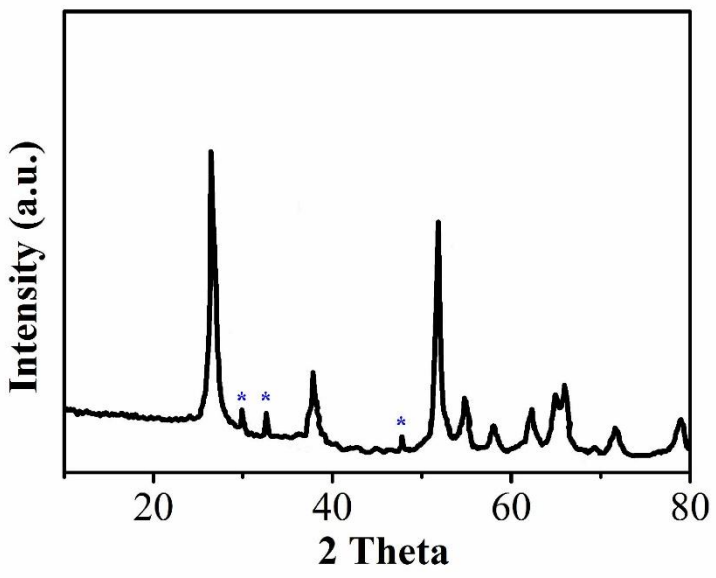

Figure 2. XRD pattern of biosynthesized SnO_2 NPs.

Figure 3 shows the FTIR spectrum of biosynthesized SnO_2 NPs. The band between 400 to 500 cm^{-1} can be assigned to Sn─O [32]. The peak located at 890, 1001, 1335, 1555 and 2360 cm^{-1}can be assigned to aromatic CH_2 out of plane bending [33-37], aromatic ring stretching of cyclic compound, N_3 symmetric stretching and stretching vibration of olefinic compounds [38], respectively. The weak absorption at 2340 cm^{-} denotes N-H stretching vibration of the secondary amine. Therefore, the biomolecules capping on the SnO_2 NPs probably are volatile essential oil and flavonoids.

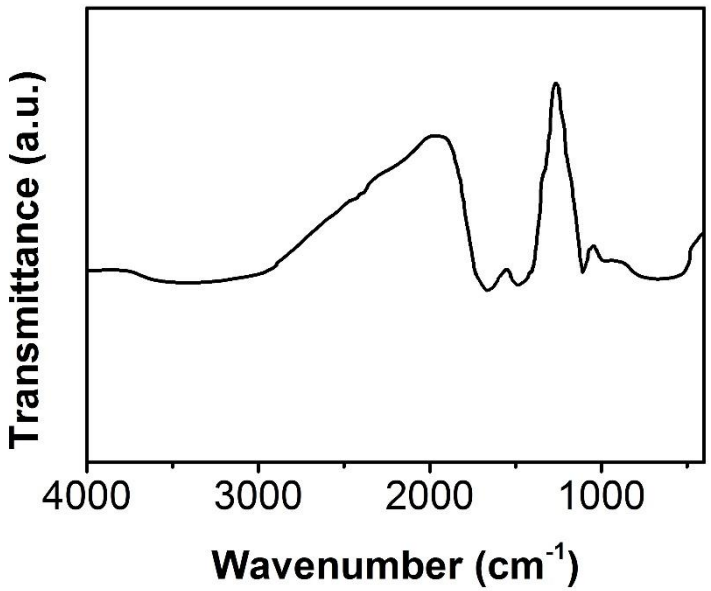

Figure 3. FTIR spectrum of biosynthesized SnO_2 NPs.

The optical properties of the biosynthesized SnO_2 NPs were also investigated by took the reflectance spectrum of biosynthesized SnO_2 spinning coated thin film. Figure 4 shows the reflectance spectrum of the SnO_2 NPs, which exhibits a strong decrease after 360 nm due to the optical transitions occurring in the optical band gap. Kubelka-Munk function has been used for determining the band gap of the biosynthesize SnO_2 NPs [39]:

$$F(\mathrm{R}) = \frac{(1-\mathrm{R})^2}{2R} = \frac{R}{S}$$

Where F(R) is the Kubelka-Munk function which corresponds to the absorbance, R is the reflectance, K is the absorption coefficient, and S is the scattering coefficient. Because the Kubelka-Munk function F(R) is directly proportional to the absorbance. Therefore, the linear absorption coefficient of α can be calculated using following equation:

$$\alpha = \frac{F(\mathrm{R})}{t} = \frac{\mathrm{Absorbance}}{t}$$

Where t is the thickness of the biosynthesized SnO_2 NPs film. Then, the $\left(\frac{F(\mathrm{R})\mathrm{hv}}{t}\right)^2$ *vs. hv* for the biosynthesized SnO_2 film was plotted (Inset Figure 4). The optical band gap was found to be 3.62 eV. Similar observations are reported by other workers [40].

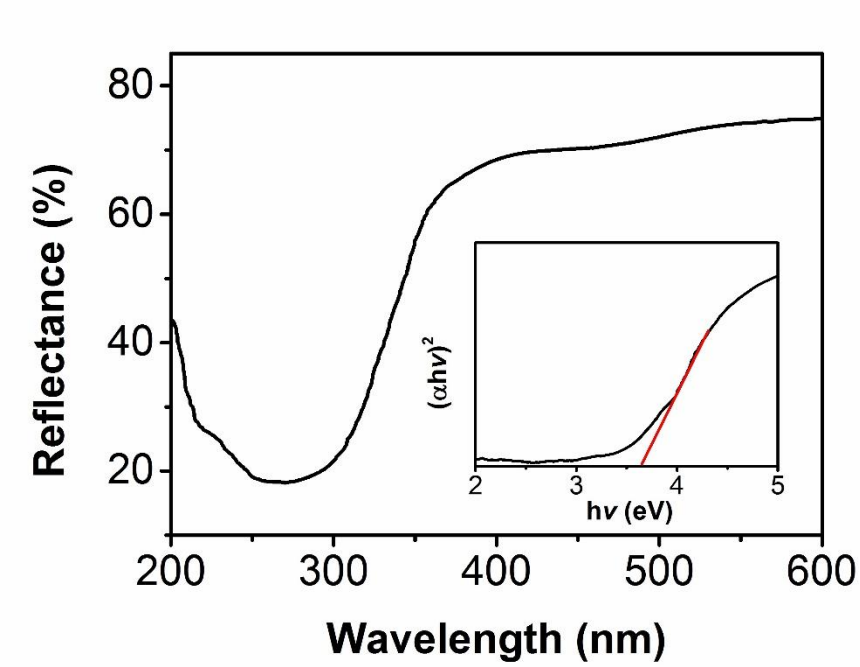

Figure 4. Reflectance spectrum of biosynthesized SnO_2 NPs. Inset: plots of $(\alpha h\nu)^2$ vs. photon energy ($h\nu$) of biosynthesized SnO_2 NPs.

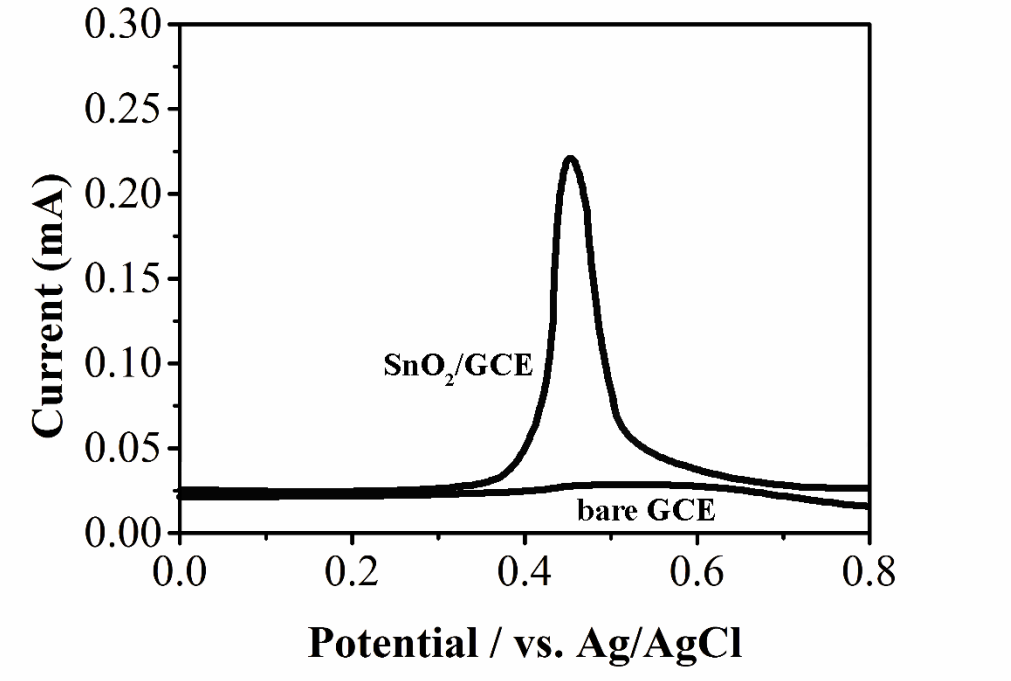

Figure 5. DPV of 0.5 μM Hg^{2+} recorded at (a) bare GCE and (b) SnO_2/GCE.

Figure 5 shows the DPV response of bare GCE and SnO_2/GCE towards detection of 0.5 μM Hg^{2+}. A small oxidation peak was observed at the potential of 0.51 V using bare GCE. On the other hand, a much bigger oxidation peak could be observed at SnO_2/GCE with peak current of 0.21 mA at potential of 0.44V. This signal increasing and negatively shifted peak potential can be ascribed by the enhanced conductivity and increased surface area provided by the biosynthesized SnO_2 NPs modified electrod.

Accumulation steps are always used for enhancing the electrochemical response of the electrode. As shown in Figure 6, we tested the accumulation potential and period in the Hg^{2+} detection. It can be seen that the peak current increases from 0 to ─0.70 V and then decreases if increasing accumulation potential. Moreover, the current also increase when the accumulation time increasing from 50 to 400 s. If further increasing the accumulation time, the current responses remain similar. Therefore, we chose accumulation conditions of ─0.70 V and 400 s for our optimization conditions.

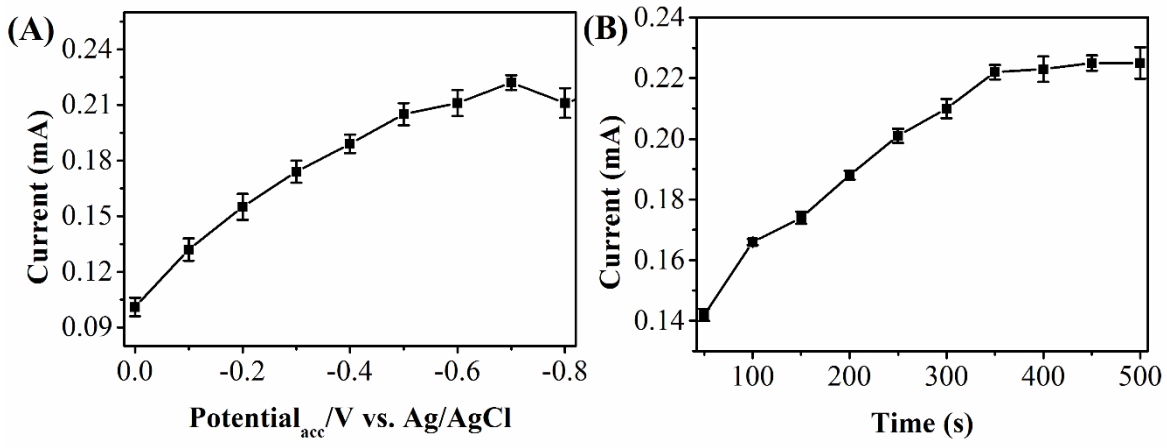

Figure 6. Influence of the (A) accumulation potential and (B) accumulation time.

For the real applications, we tested the response time, linear range and detection limit of our proposed electrode. Figure 7 displays an amperometric responses of SnO_2/GCE to Hg^{2+} at concentrations from 0.001 μM to 1.5 μM at a working potential of 0.7 V. As shown in figure, our proposed SnO_2/GCE showed a linear detection range from Hg^{2+} concentrations 0.001 μM to 1.5 μM. Moreover, the amperometric figure showed the SnO_2/GCE could reach steady-state within 3s after addition of Hg^{2+}, indicating the proposed SnO_2/GCE had a quick response time. The linear regression equation was calculated as: I_{pa} (μA) = 0.611234 c (nM) + 51.8755 (R^2 = 0.99). The detection limit for Hg^{2+} is calculated to be 0.3 nM. This such excellent performance can be ascribed to the specific role of biosynthesized SnO_2 nanoparticles. The biosynthesized SnO_2 nanoparticles not only provide a larger surface area for Hg ions adsorption but also could electrocatalytic oxidation of Hg ions. Moreover, the biosynthesized SnO_2 may contain some bio-molecules, which could form Hg ions-SnO_2 complex. The formed complex could more sensitive in electrochemical condition to provide a strong signal.

The interference study is very important before using the electrode for real applications. We tested common interferences in the drinking water at the SnO_2/GCE. The results indicated that the 25-

fold of Na^+, K^+, Pd^{2+}, Co^{2+}, Cl^- and I^- did not interfere the test results, indicating our proposed electrode owing an excellent selectivity.

The feasibility of proposed Hg^{2+} sensor for water sample analysis were also conducted. We chose tap water, lake water, rain water and bottle as test samples. The sample was directly spiked with certain amounts of Hg^{2+} standard solution. Hg^{2+} was measured by standard addition method in the real sample. The test results were summarized in Table 1.

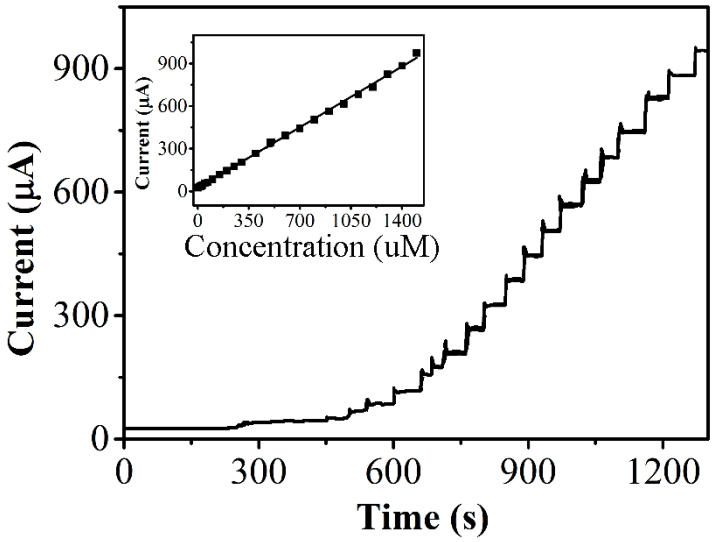

Figure 7. Amperometric response of the SnO_2/GCE. Applied potential: 0.7 V. Inset: The calibration curve for Hg^{2+} detection using SnO_2/GCE.

Table 1. Determination of Hg^{2+} in water samples using ZnO-RGO/ITO.

Sample	Added (nM)	Found (nM)	Recovery (%)	RSD (%)
Tap water 1	0	0	—	0.15
Tap water 2	20	19.32	94.2	1.11
Rain water 1	50	50.02	101.4	1.22
Rain water 2	100	99.10	101.1	3.78
Bottle water 1	200	199.31	99.11	2.55
Bottle water 2	500	498.87	99.62	1.34
Lake water 1	500	503.54	101.2	2.25
Lake water 2	1000	1000.44	102.11	1.78

As shown in above, the real sample analysis revealed that the recovery of sensor was in the range of 94.2–102.11%, indicating that the SnO_2/GCE is capable for accurate detecting Hg^{2+} in various water samples.

4. CONCLUSION

Green synthesis of spherical SnO_2 NPs with an average size of 132 nm has been achieved using leaf extract of *Ficus carica*. Characterizations indicated that this green, inexpensive, pollution free and eco-friendly approach could yield a high quality SnO_2 NPs. The prepared SnO_2 NPs was then used as electrode modifier for electrochemical determination of Hg^{2+}. The SnO_2/GCE exhibited a linear relationship with in the Hg^{2+} concentration range from 0.001 to 1.5 μM. Our proposed Hg^{2+} sensor also exhibits excellent stability and feasibility.

Reference

1. Y. Konishi, K. Ohno, N. Saitoh, T. Nomura, S. Nagamine, H. Hishida, Y. TakahashiandT. Uruga, *J. Biotechnol.*, 128 (2007) 648
2. S.K. Das, C. Dickinson, F. Lafir, D.F. BroughamandE. Marsili, *Green Chemistry*, 14 (2012) 1322
3. H. Abdul Salam, R. SivarajandR. Venckatesh, *Materials Letters*, 131 (2014) 16
4. G. Sangeetha, S. RajeshwariandR. Venckatesh, *Mater. Res. Bull.*, 46 (2011) 2560
5. S. NagarajanandK.A. Kuppusamy, *Journal of Nanobiotechnology*, 11 (2013)
6. P. Rajiv, S. RajeshwariandR. Venckatesh, *Spectrochimica acta. Part A, Molecular and biomolecular spectroscopy*, 112 (2013) 384
7. R. Yuvakkumar, J. Suresh, A.J. Nathanael, M. SundrarajanandS.I. Hong, *Mater. Sci. Eng., C*, 41 (2014) 17
8. B. Ajitha, Y. Ashok Kumar ReddyandP. Sreedhara Reddy, *Spectrochimica Acta Part A: Molecular and Biomolecular Spectroscopy*, 128 (2014) 257
9. C. Jayaseelan, R. Ramkumar, A.A. RahumanandP. Perumal, *Industrial Crops and Products*, 45 (2013) 423
10. R. Von Hagen, M. SnehaandS. Mathur, *Journal of the American Ceramic Society*, 97 (2014) 1035
11. J. Zhao, W. Shan, X. Xia, Q. WangandL. Xing, *Sci. China Technol. Sci.*, 57 (2014) 1081
12. Y. Liu, Y. Jiao, S. Zhang, B. Yin, F. QuandX. Wu, *Sci. Adv. Mater.*, 6 (2014) 1184
13. L. Fu, W. Cai, A.W. Wang, Y.H. Zheng, L. HeandZ.X. Fu, *Mater. Technol.*, 30 (2015) 264
14. Y. Zheng, A. Wang, H. Lin, L. FuandW. Cai, *RSC Advances*, 5 (2015) 15425
15. Y. Zheng, L. Fu, A. WangandW. Cai, *Int. J. Electrochem. Sci*, 10 (2015) 3530
16. Z. Wen, D. Lu, S. Li, J. SunandS. Ji, *Int. J. Electrochem. Sci*, 9 (2014) 1
17. A. Elzatahry, *Int. J. Electrochem. Sci*, 9 (2014) 22
18. S. Liu, G. Huang, J. Yu, T.W. Ng, H.Y. YipandP.K. Wong, *ACS Appl. Mater. Interfaces*, 6 (2014) 2407
19. Y.-C. Chang, C.-Y. YanandR.-J. Wu, *J. Chin. Chem. Soc.*, 61 (2014) 345
20. Q. GuoandX. Qin, *J. Solid State Electrochem.*, 18 (2014) 1031
21. X. Wang, S. Qiu, J. Liu, C. He, G. LuandW. Liu, *European Journal of Inorganic Chemistry*, 2014 (2014) 863
22. L. Fu, Y. Zheng, A. Wang, W. CaiandH. Lin, *Food chemistry*, 181 (2015) 127
23. J.M. Roller, H. Yu, L. Zhang, P. Plachinda, M.B. Vukmirovic, S. Bliznakov, M. Li, R.R. AdzicandR. Maric, *Microsc. Microanal.*, 20 (2014) 462

24. Y.-C. Her, B.-Y. YehandS.-L. Huang, *ACS Appl. Mater. Interfaces*, 6 (2014) 9150
25. X. Wang, C. Zhao, R. LiuandQ. Shen, *Journal of Nanoparticle Research*, 16 (2014) 1
26. R.K. Mishra, A. KushwahaandP.P. Sahay, *J. Exp. Nanosci.*, (2014) 1
27. N. YongvanichandS. Maensiri, *Integrated Ferroelectrics*, 156 (2014) 53
28. V. Sahu, S. Lalwani, G. SinghandR.K. Sharma, *Advanced Science Letters*, 20 (2014) 1369
29. N. SrivastavaandM. Mukhopadhyay, *Ind. Eng. Chem. Res.*, 53 (2014) 13971
30. L. Fu, W. Cai, A. WangandY. Zheng, *Materials Letters*, 142 (2015) 201
31. B. Ulug, M. Haluk Turkdemir, A. CicekandA. Mete, *Spectrochimica acta. Part A, Molecular and biomolecular spectroscopy*, 135 (2015) 153
32. H. Yang, Z. Hou, N. Zhou, B. He, J. CaoandY. Kuang, *Ceram Int*, 40 (2014) 13903
33. M.Z. Hussein, W.H.W.N. Azmin, M. MustafaandA.H. Yahaya, *Journal of Inorganic Biochemistry*, 103 (2009) 1145
34. L. FuandZ. Fu, *Ceram Int*, 41 (2015) 2492
35. L. Fu, Y. Zheng, Q. Ren, A. WangandB. Deng, *Journal of Ovonic Research*, 11 (2015) 21
36. L. Fu, Y. ZhengandA. Wang, *Int. J. Electrochem. Sci*, 10 (2015) 3518
37. L. Fu, Y. Zheng, A. Wang, W. Cai, Z. FuandF. Peng, *Sensor Letters*, 13 (2015) 81
38. S. Maensiri, P. LaokulandV. Promarak, *Journal of Crystal Growth*, 289 (2006) 102
39. V. Senthilkumar, P. VickramanandR. Ravikumar, *J. Sol-Gel Sci. Technol.*, 53 (2010) 316
40. B.-J. Huang, F. Li, C.-W. Zhang, P. LiandP.-J. Wang, *J. Phys. Soc. Jpn.*, 83 (2014) 064701